JOINT INSTITUTE FOR NUCLEAR RESEARCH
Laboratory of Nuclear Problems

FINAL REPORT ON THE INTEREST PROGRAMME

Evaluation of the radiation effects on advanced materials exposed to electron beam and gamma rays using the Raman Spectroscopy

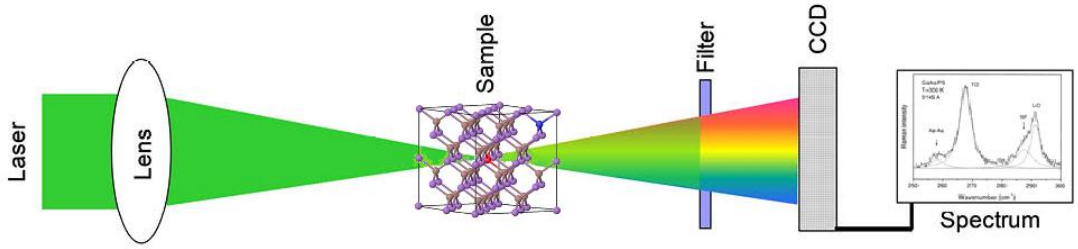

Supervisor:
Dr. Antonio Leyva Fabelo

Student:
Solné Reyes Peña, Cuba
Higher Institute of Technologies and Applied Sciences, at Havana University

Participation period:
8 February - 19 March, Wave 3

Dubna, 2021

Abstract

A 300 μm thick GaAs:Cr detector was irradiated with 20 MeV electrons on the LINAC-800 accelerator, and measured its Raman spectra on the incident and exit surfaces, before and after irradiation, in order to evaluate the radiation damage in the material. The LO and TO peaks were evidently seen in all cases. The obtained Raman spectra exhibited significant differences in the input surface before and after the irradiation, as the slight change in the frequency position of the main modes to lower values, and the severe suppression of the high frequencies tail of the LO peak. Through the deconvolution procedure, it was possible to identify several vibrational and coupling modes present in the semiconductor material, such as the SO and the L^+ and L^- peaks, accountable for the broadening and asymmetrical shape of the central peak. The analysis of the behaviour of the longitudinal optical phonon-plasmon coupling led to the conclusion that the charge carrier concentration in the target, decreased after the electron´s exposure. Additionally, the red shifting of the main optical modes implied a modification of the tensional state of the crystalline structure. On the other hand, the spectra of the output surface did not showed such marked variations because of the attenuation of the electrons beam in the bulk material.

Introduction

Man has created many types of radiation detectors for the most diverse purposes, and among all, those manufactured with semiconductor materials stand out due their numerous advantages. There are many semiconductor materials used for this purpose, for example: Si, Ge, CdTe, CdZnTe, HgI_2, GaAs, etc. However, in recent years the chromium compensated gallium arsenide (GaAs:Cr) has been in the scope of many laboratories due to its outstanding properties that make it one of the candidates with more perspectives in applications for High Energy Physics and Medical Physics.
Some of these properties are it high Z, good detection efficiency, high charge carrier mobilities, low noise, the possibility of operating at room temperature [1] and high resistance to radiation damage [2].
Knowing that the detector's performance strongly depends on the device material's structural and electronic properties, and these properties can be affected when exposed to ionizing radiation, then is understood the importance of studying the effect of radiation on the material.
On the basis of this fact, we precisely have selected the GaAs:Cr semiconductor as the target of this research, aimed at deepening the knowledge of the effects of radiation of 20 MeV electrons on its structure, using for them the Raman spectroscopy as a fundamental tool.

Materials and methods

Raman spectroscopy

Raman spectroscopy is a spectroscopic technique used to develop a qualitative and quantitative analysis of almost any material. It is typically applied to determine vibrational modes of molecules, although rotational and other low frequency modes of systems may also be observed. Among its major advantages are that there is no need of preparation of the sample of study and it is a non-destructive technique [3]
Raman spectroscopy is based in the Raman effect which was discovered by the Indian physicist Chandrasekhra Venkata Raman in 1928. Simply stated, the Raman effect can

be described as the inelastic scattering of light by matter. When a photon of visible light, too low in energy to excite an electronic transition, interacts with a molecule it can be scattered in one of three ways. It can be elastically scattered and thus retain its incident energy, known as Rayleigh scattering, or it can be inelastically scattered by either giving energy up to, or by removing energy from, the molecule. Photons undergoing inelastic loss of energy give rise to Stokes scattering whilst photons undergoing inelastic gain of energy give rise to anti-Stokes scattering. The energy gained by the molecule in Stokes scattering appears as vibrational energy and where a molecule has excess vibrational energy above the ground state, it is this energy which is lost to the anti-Stokes scattered photons. In figure 1, are represented the energy level diagram corresponding to the Raman effect.

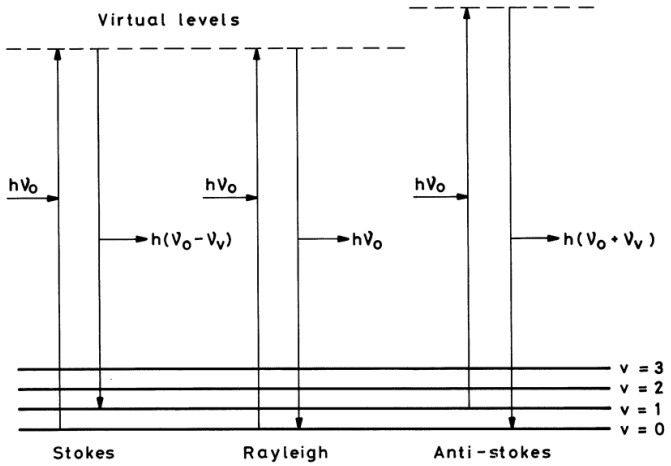

Figure 1. Quantised model of Rayleigh scattering and Stokes and anti-Stokes Raman scattering [4].

The Rayleigh scattering arises from transitions which start and finish at the same vibrational energy level. Stokes Raman scattering arises from transitions which start at the ground state vibration al energy level and finish at a higher vibrational energy level, whereas anti-Stokes Raman scattering involves a transition from a higher to a lower vibrational energy level.

Details of the phenomenon can be found, for example, in [4].

In a typical experimental setup for Raman measurement, a sample is illuminated with a source of monochromatic light, this light interacts with molecular vibrations, phonons or other excitations in the system, resulting in the energy of the photons being shifted up or down. The shift in energy gives information about the vibrational modes in the system. Electromagnetic radiation from the illuminated spot is collected with a lens and sent through a monochromator. Elastic scattered radiation at the wavelength corresponding to the source line is filtered out by either a notch filter, while the rest of the collected light is dispersed onto a detector.

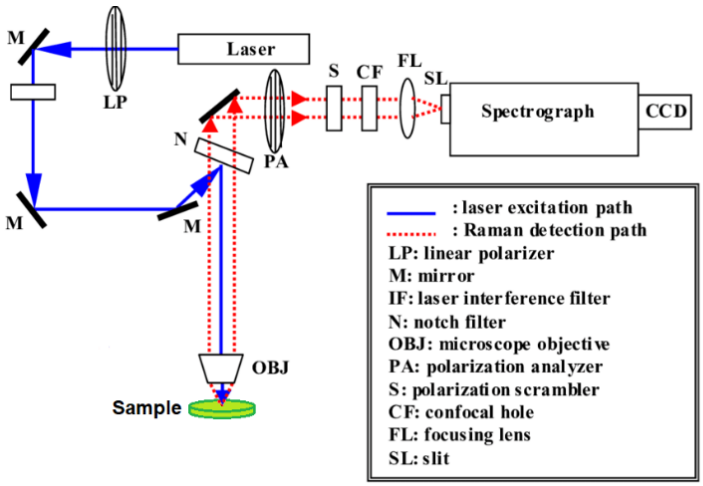

Figure 2. Schematic of the backscattering geometry in Raman spectrometer.

There are several experimental configurations used in Raman spectroscopy, highlighting the backscattering geometry (135° or 180°), which has several advantages over the commonly used 90° scattering geometry [5]. In figure 2 is presented schematic of the backscattering geometry in Raman spectrometer. In this investigation the measurements were made in a spectrometer model CARS Solar TII, and applying the following conditions: diffraction grating of 1200 lines/mm, objective 40x (model Olympus-UPlanFL N), and acquisition time 70 s.

GaAs:Cr

The GaAs is a semiconductor composed of two sublattices, each face centered cubic (fcc) and offset with respect to each other by half the diagonal of the fcc cube. This crystal configuration is known as cubic sphalerite or zinc blende [6].
The GaAs material has a resistivity greater than 10^7 Ω*cm at room temperature and carriers mobilities of the order μe ~ 10^3 $cm^2/V*s$ and μh ~ 10^2 $cm^2/V*s$ for electrons and holes respectively [7]. The density of GaAs is of 5.32 g/cm^3, which offers an advantage over traditional semiconductors such as Si, mainly for highly penetrating radiation.
Despite the advantageous properties of GaAs, it has a high concentration of traps in the material that have until now limited its spectroscopic resolution [8]. The ionized EL2 defect ($EL2^+$) is a highly efficient recombination center due to its large electron trap cross section, limiting the electron's lifetime to values of the order of 1 ns, reducing the drift path of electrons, and resulting in detectors with poor charge collection efficiency and low spectroscopic performance. It is then of most importance decrease the EL2+ concentration in order to make GaAs an adequate radiation detector material.
There are several methods to reduce the $EL2^+$ centers concentration in the GaAs material [9], but we will refer to only one for its superiority and for being the one used to grow our target. In this method the initial GaAs material is developed with an excess of shallow donors, becoming an n-type material with an electron concentration of about 10^{17} cm^{-3}. Then Cr is evaporated onto the GaAs and thermally diffused into the bulk [8]. The chromium diffusion generates interstitial defects in the crystal structure before becoming fixed in the Ga vacancies, producing a deep acceptor trap at 0.78 eV above the valence band. The excess shallow donors present in the initial material fill the ionized $EL2^+$ states, producing the neutral $EL2^0$ and partially compensate the Cr_{Ga} traps. The resulting highly compensated p-type material has high resistivity (ρ ~ 10^9 Ω*cm) and good charge carrier transport (μ_e ~ 4000 $cm^2/V*s$ and μ_h ~ 300 $cm^2/V*s$), allowing the production of active layers of GaAs:Cr up to 1 mm of thickness [7].
In figure 3 a representation of the GaAs:Cr supercell is shown.

The parameters of the detectors based on semi-insulating gallium arsenide compensated with chromium (GaAs:Cr) are radically different; the resistivity of this material is two orders of magnitude higher than that of undoped GaAs, and for GaAs:Cr, the current–voltage characteristics are nearly linear, in contrast to the devices based on undoped GaAs [7].
In figure 4 the photo of high resistivity GaAs:Cr detector employed as the target in this work experiment is presented. This is a 300 μm thick sensor with an area of 4.5 x 4.5 mm^2 and a 1 μm thick nickel square shape anode (1.8 x 1.8 mm^2 area) on the center of surface (input surface).

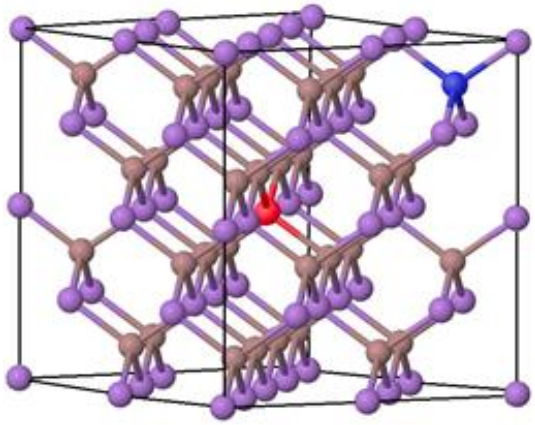

Figure 3. Representation of GaAs:Cr supercell. The Ga, As, Cr and Te atoms are identified by violet, brown, red and blue spheres respectively.

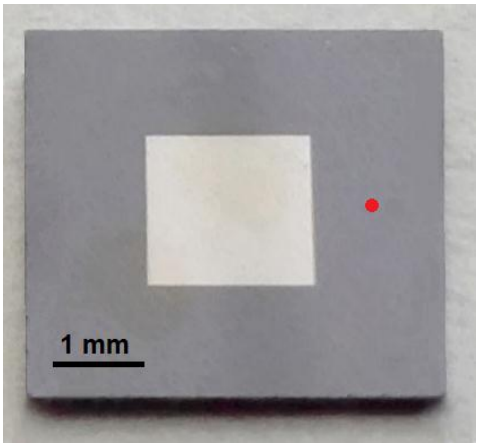

Figure 4. Photo of the target. The red circle to the right of the electrode shows a typical location of the laser spot from Raman spectrometer.

LINAC-800

The irradiation of the studied sample took place in the electron linear accelerator LINAC-800 from the Nuclear Problems Laboratory at the Joint Institute of Nuclear Research (LNP-JINR). Figure 5 shows a schematic representation of the installation.

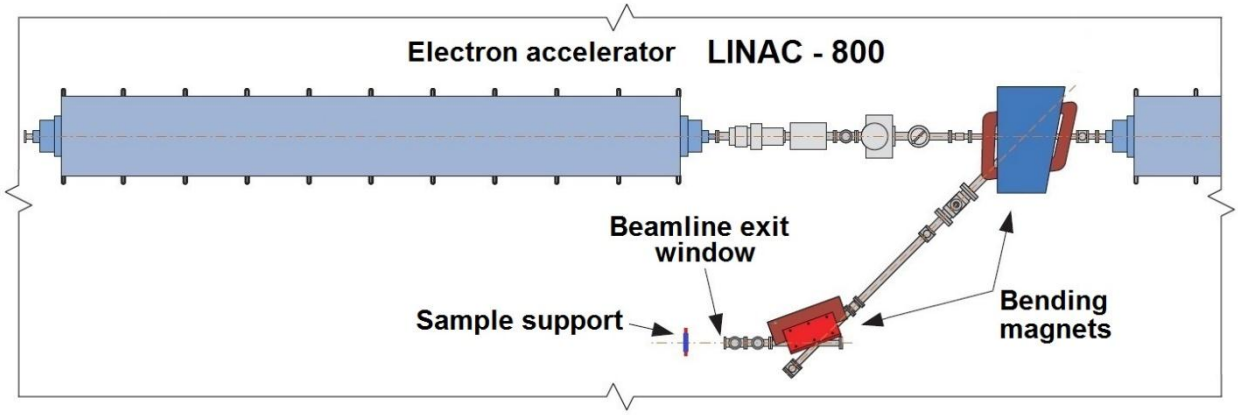

Figure 5. Schematic view of the LINAC- 800 accelerator.

The irradiation took place at room temperature, perpendicular to the surface where the detector has the Ni electrode, covering the entire sample. The beam characteristics were: energy of the electrons E_{e^-} = 20 MeV, current intensity I = 10 mA, frequency f = 10 Hz, pulse length Δt = 1.5 μs, total irradiation time T_{irrad} = 30 min. The estimation of the total fluence in the irradiated sample resulting in $\Phi = 1.8643 \times 10^{14}$ e^-/cm^2.

Deconvolution method

The deconvolution of the Raman spectra was performed in the interval between 260 and 325 cm^{-1} using the full width at half maximum (FWHM) version of the Gaussian function, defined by the equation:

$$y = y_0 + \frac{Ae^{\frac{-4\ln(2)(x-x_C)^2}{w^2}}}{w\sqrt{\frac{\pi}{4\ln(2)}}}, \quad (4)$$

where y_0 is the base, A is the area of the peak, x_c is the position of the center of the peak, and w is the FWHM [10].
For these purposes was used the OriginPro 8 software.

Results

Determination of the measurement effective depth

If on the surface of a medium hits a parallel beam of light of intensity I_0 a reduction of this light intensity will occur according to the Bouguer-Beer-Lambert law:

$$I = I_0 e^{-\alpha z}, \quad (1)$$

where I is the intensity of light at depth z and α the absorption factor. The value of this coefficient represents the thick of the layer at which the wave intensity is diminished e times, to a 36.8 % of the original intensity.
On the other hand, it is well known that the amplitude E of a plane wave moving in the z direction, in an absorbing medium behaves as:

$$E(z,t) = E_0 e^{i(kz-\omega t)} = E_0 e^{i(\frac{2\pi}{\lambda_0}nz-\omega t)} = E_0 e^{-\frac{2\pi}{\lambda_0}\kappa z} e^{i(\frac{2\pi}{\lambda_0}\eta z-\omega t)}, \quad (2)$$

where the diffraction index $n = \eta + i\kappa$ is now a complex number, being its imaginary component the extinction coefficient, which accounts for the damping of the light wave in the absorbing medium, E_0 the initial amplitude of the light electric field, λ_0 its wavelength and k and ω are the wavenumber and angular frequency respectively.
Stated this and remembering that the intensity of the wave is proportional to the square of its amplitude, the absorption factor will be:

$$\alpha = \frac{4\pi}{\lambda_0}\kappa, \quad (3)$$

The distance in the medium at which the light intensity reaches a $1/e^2$ fraction (approximately 13.5%) of its original value, is considered as the sensible depth of the technique. In our experiment the wavelength of the He-Ne laser is λ_0 = 632.8 nm and the value of the extinction coefficient for the GaAs:Cr in this wavelength range is κ = 0.18932, resulting in a characteristic penetration depth (2/α) of 532.0 nm.

Primary intercomparative analysis of the spectra

The spectra of the studied target input surface before and after irradiation are presented in figure 6. From the superposition of them can be observed some important differences. In both Raman spectra we can see the presence of an intense central peak at ~ 292 cm^{-}

[1], the longitudinal optical (LO) Ga-As phonon mode, which agrees with the experimental and calculated results reported in [11].

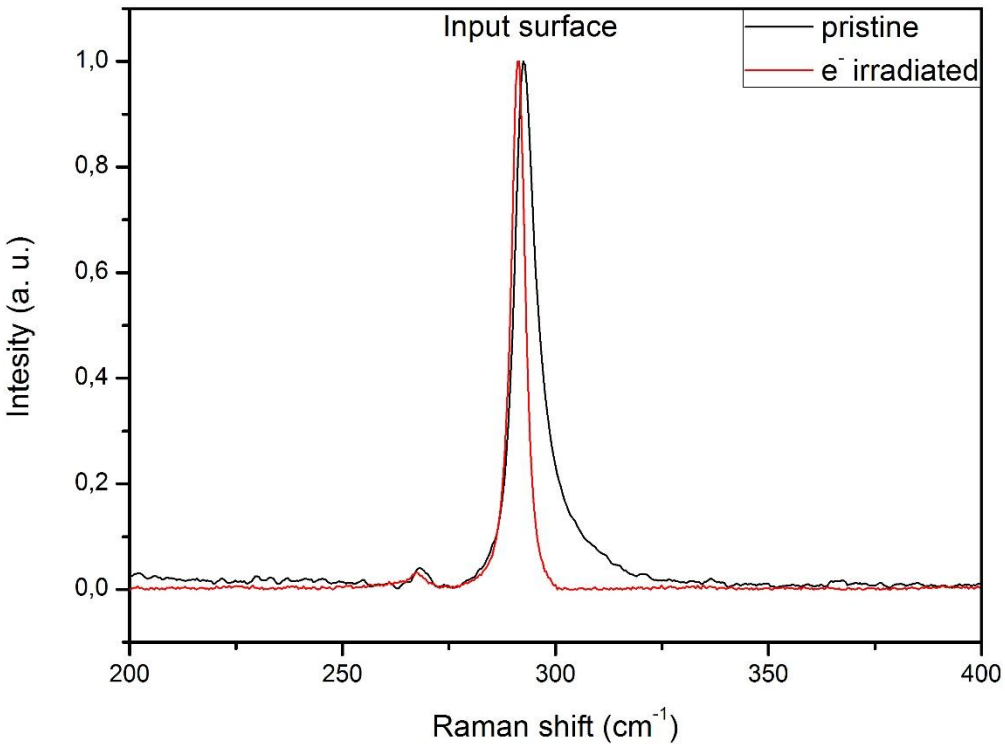

Figure 6. Raman spectra of the GaAs:Cr input surface before and after the electron irradiation.

In addition, there is a low intensity mode observed at ~ 268 cm^{-1}. This vibration can be attributed to the transverse optical (TO) Ga–As phonon mode, forbidden by the selection rules for Raman scattering, but probably presents as a consequence of the violation of symmetry in the sample for the existence of a small amount of disoriented crystals in the material [12].

It is apreciable the asymmetric shape of the LO peaks, specially marked, as a tail to higher frequencies, in the unirradiated case. This asymmetry is the result of the presence of complementary vibrational modes due the coupling between the LO phonons and the charge carriers plasmons, and occurrence at higher frequencies of longitudinal Cr-As and Cr-Ga vibrations [13] [14].

The observed shift of peaks to lower frequencies positions as a consequence of the irradiation with electrons are not too severe, indicating probably the slight altering of the vibrational and tensional states of the crystalline structure.

It is also worth notice the slight dominance of the background intensity of the nonirradiated spectrum over the irradiated case. This could be due to the presence of vibrational modes related to the existence of As-clusters resulting from the crystal synthesis process [15]. After the irradiation, this low-frequency background anomaly is quite suppressed, possibly due to relaxations in the structure because of the radiation damage.

Figure 7 shows the measured spectra on output sides of the sample before and after irradiation. Clearly, the effect of the radiation with 20 MeV electrons is much less marked on the output side, or opposite to the incidence. After exposure, the spectrum corresponding to the output side changes slightly only in the region of the high frequencies of the peak identified as LO; neither the positions nor the intensity ratio of the

TO and LO modes are hardly affected. This is an expected behavior that reflects the lower amount of radiation damage in the area sensitive to the method in the region adjacent to the target exit surface, a consequence of the scattering and absorption phenomena of the electron beam while passing through the medium. The background noise of the spectra is marked for both cases.

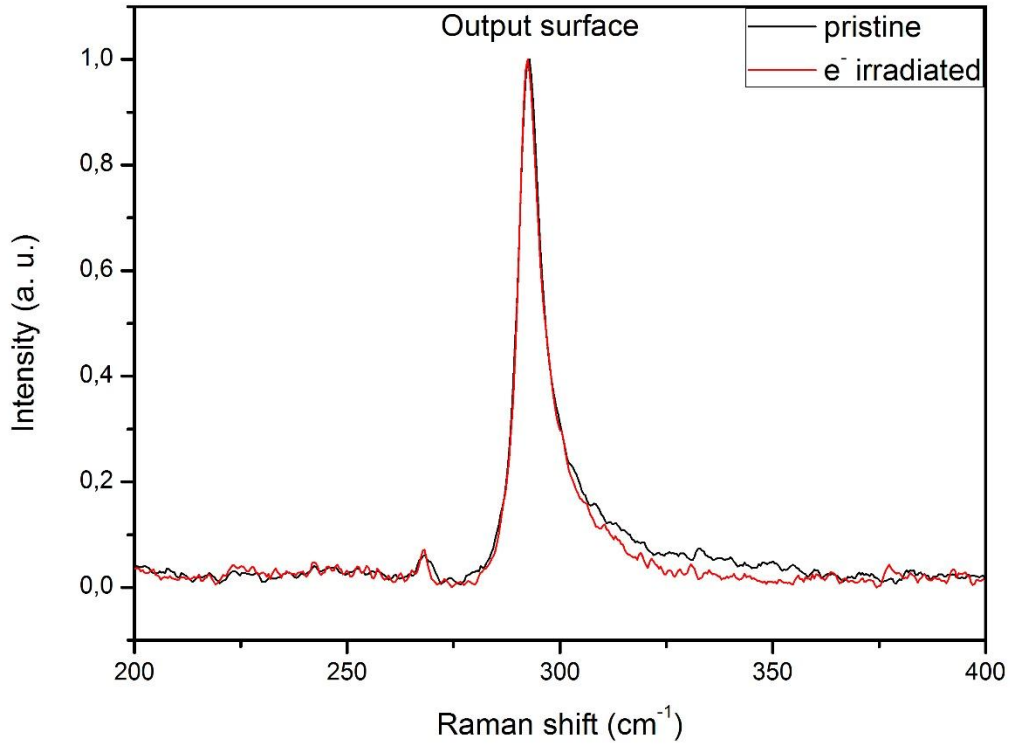

Figure 7. Raman spectra of the GaAs:Cr output surface before and after the electron irradiation.

Analysis of the deconvoluted spectra

The detailed analysis of the previous spectra is carried out with the use of mathematical deconvolution in the Raman shift interval between 260 and 325 cm^{-1}, the most interesting. We will pay attention only to the spectra from the sample surface directly exposed to radiation, where the effects are evident.

Table 1 shows a resume of the characteristics of the most important peaks from the Raman spectra take at the input surface before and after electron irradiation, and the fitting parameters used to validate the deconvolution, R^2 and χ^2.

Figure 8 shows the spectrum deconvolution of the input surface in the range of interest. Optical modes TO and LO are easily identified appearing in the expected positions. The presence of a peak with very low intensity in the position coinciding with those of the surface optical mode (SO) in GaAs is also seen.

A couple peaks identified as L^+ and L^- are present in the plot. These are the electrostatic coupling of LO phonons with the surrounding carrier plasmons resulting in the formation of LO phonon-plasmon coupled modes (LOPC), also called plasmarons, which can mediate the carrier lattice energy exchange and thus play an important role in the electrical characteristics of semiconductor-based devices [16].

Table 1. Mean characteristics of the deconvoluted spectra.				
Characteristic	**Mode**	**Non-irradiated**	**Irradiated**	**Frequency position displacement (cm^{-1})**
Raman shift (cm^{-1})	TO	268.4379	267.5786	0,8593
	LO	292.4071	291.2390	1,1681
	SO	283.4500	284.3538	-0,9038
	L^-	264.4085	263.4308	0,9777
	L^+	294.2957	291.2416	3,0541
Raman intensity (a. u.)	I_{TO}	0.0401	0.0290	
	I_{LO}	0.5621	0.6732	
	I_{SO}	0.0201	0.0246	
	I_{L^-}	0.0091	0.0114	
	I_{L^+}	0.4754	0.3290	
FWHM (cm^{-1})	TO	4.3322	5.4430	
	LO	4.0995	3.0494	
	SO	9.9629	10.5870	
	L^-	1.5966	2.1091	
	L^+	10.4549	6.9962	
Adjusted R^2		0.9997	0.9995	
Reduced χ^2		1,65969E-5	1,92267E-5	

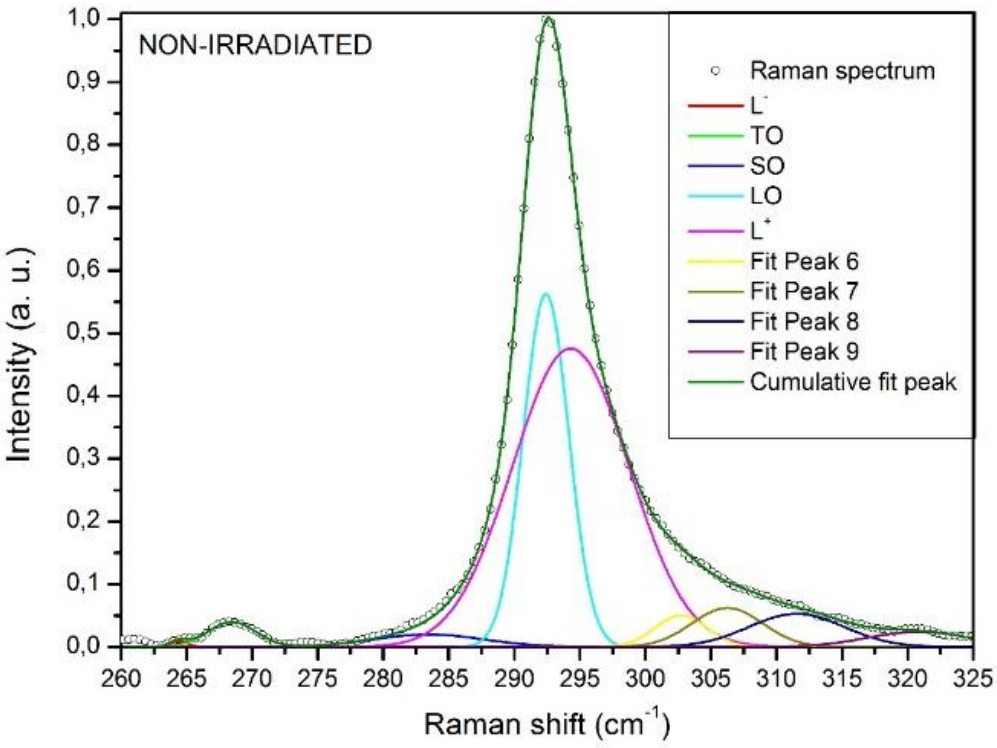

Figure 8. Raman spectrum deconvolution from the non-irradiated input surface.

The mode at a frequency of 294.3 cm^{-1} can be identified as the LOPC L^+, and the one at 264.4 cm^{-1} L^-. As is possible to observe in figure 8, mode L^+ is the most important contributor to the asymmetric broadening of the LO peak. The greater intensity and semi-

width of the L^+ peak with respect to L^- is noteworthy. It is widely reported in the literature that the positions of these peaks are highly dependent on the concentration of free carriers and the wavelength of the laser, therefore they can be used to estimate these parameters in the semiconductor [17, 18].
Above 300 cm^{-1}, deconvolution shows the possible presence of 4 peaks, which obviously together with L^+ are the main responsible for the marked asymmetry with broadening towards the high frequencies of the most intense peak of the spectrum. A similar behavior was reported in [19], where the authors associate this result with the absorption characteristics of laser light in an opaque semiconductor, and the influence of the high surface recombination rate, which leads to electron-hole plasma inhomogeneity. The electric interaction of the mentioned optic phonons with this inhomogeneous plasma could be the cause of this complicated spectrum.
The deconvoluted Raman spectra corresponding to the input surface after the electron irradiation is shown in figure 9.

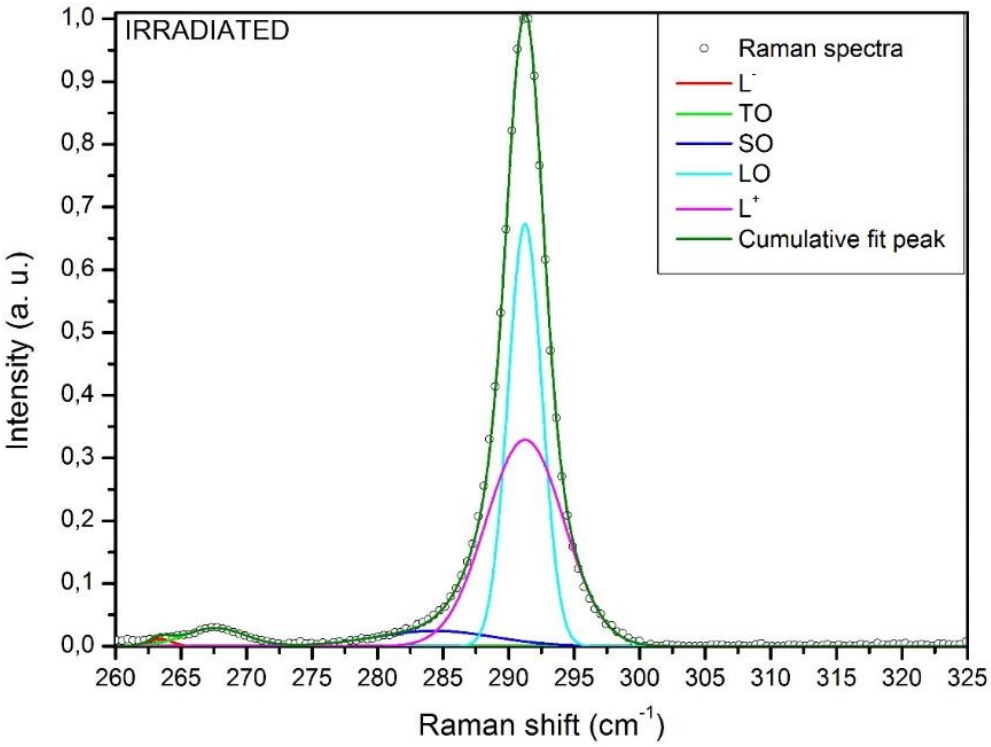

Figure 8. Raman spectrum deconvolution from the irradiated input surface.

The most significant feature of this case is the almost total disappearance of the last four peaks, that is, those that appear at the highest frequencies. This phenomenon together with the red shift of both LOPC modes, 0.98 cm^{-1} and 3.05 cm^{-1} for L^- and L^+ respectively, may indicate a weakening in the coupling between the optical phonons and the plasmon because of the decrease in the free charge carrier concentration. It is well known that as the free charge carrier concentration increase, the separating gap between L^+ and L^- becomes greater. In this experiment, this quantity goes from 29.9 cm^{-1} in the pristine sample to 27.8 cm^{-1} after the irradiation with electrons, thus indicating the decrease of the charge carrier concentration.
The deconvolved Raman spectrum also shows a red shift in the frequency positions of the TO and LO modes after the electron irradiation. This shift could be due to the improved

crystallinity of the material, thought of as certain relaxation of the stress present in the structure.
Finally, it is interesting to note the displacement of the SO mode to higher frequencies. This fact and its relationship with radiation damage is still under study.

Conclusions

The qualitative and quantitative analysis of the Raman spectra corresponding to the input and output surface of a 300 µm thick GaAs:Cr detector, before and after the irradiation of with 20 MeV electrons beam, were performed. The intercomparative analysis of the spectra obtained for the radiation input surface in the sample before and after being irradiated showed significant changes caused by the action of the electrons from the beam. However, on the output face this effect was not significant due to the electron beam attenuation in the sample´s medium. The deconvolution procedure applied to the spectra made it possible to identify, in addition to the expected optical peaks of GaAs: Cr TO, LO and SO, two LO phonon-plasmon coupling modes, L+ and L-, as well as four more modes in higher frequency positions. It was possible to explain which are the modes that influence the strong asymmetry of the peak of greater intensity, and that they cease to have a contribution when the target is irradiated. The analysis of the displacement of the LOPC peaks, which takes place towards lower frequencies, allows us to conclude that, as a consequence of irradiation, the concentration of free charge carriers in the material decreases. Furthermore, the redshift behaviour of the TO and LO modes may imply a rearrangement in the semiconductor crystal structure towards less stressed configurations, stimulated by radiation damage caused by electron projectiles.

References

[1] A. Šagátová, B. Zaťko, V. Nečas, et al. From Single GaAs Detector to Sensor for Radiation Imaging Camera, Applied Surface Science, **461**, 3, (2018).

[2] K. Afanaciev, M. Bergholz, P. Bernitt, et al. Investigation of the radiation hardness of GaAs sensors in an electron beam, J. Instrum. **7**, P11022, (2012).

[3] J. Otero, y V. Gutierrez Cano. Espectroscopía Raman: Fundamento y aplicaciones. The University of Edinburgh. UK. (2015).

[4] D.J. Gardiner. Practical Raman spectroscopy. Springer-Verlag. (1989).

[5] J. R. Ferraro, K. Nakamoto and C. W. Brown. Introductory Raman Spectroscopy. Second edition. Academic Press, (2003).

[6] S. Kayali, G. Ponchak, R. Shaw. GaAs MMIC Reliability Assurance Guideline for Space Applications. JPL Publication 96-25, Chapter 3. December 15, 1996. National Aeronautics and Space Administration. Jet Propulsion Laboratory California Institute of Technology, Pasadena, California. (1996).

[7] A .V. Tyazhev, D.L. Budnitsky, O. B. Koretskay, et. al. GaAs radiation imaging detectors with an active layer thickness up to 1 mm. Nuclear Instruments and Methods in Physics Research A, **509**, 34, (2003).

[8] M. C. Veale, S. J. Bell, D. D. Duarte, et. al. Chromium Compensated Gallium Arsenide detectors for X-ray and gamma-ray spectroscopic imaging. Nuclear Instruments and Methods in Physics Research A, **752**, 6, (2014).

[9] C. Erd, A. Owens, G. Brammertz, et. al. Hard X-ray test and evaluation of a prototype 32 x 32 pixel gallium-arsenide array. Nuclear Instruments and Methods in Physics Research A, **487**, 78, (2002).

[10] W. R. Leo. Techniques for Nuclear and Particle Physics Experiments, Chap. 4, Statistics and the Treatment of Experimental Data, Springer-Verlag, (1994).

[11] W. A. Harrison. Electronic structure and the properties of solids: The Physics of the Chemical Bond, Freeman and Company, (1980).

[12] S. Mishra, D. Kabiraj, A. Roya, et al. Effect of high-energy light-ion irradiation on SI-GaAs and GaAs:Cr as observed by Raman spectroscopy. J. Raman Spectroscopy, **43**, 344, (2012).

[13] G. Abstreiter, M. Cardona and A. Pinczuk. Light Scattering in Solids IV, Springer-Verlag. Mir, (1984).

[14] P. V. Seredin, A. V. Fedyukin, I. N. Arsentyev, et al. Structural and Optical Properties of GaAs (100) with a Thin Surface Layer Doped with Chromium. Semiconductors. **50**, 853, (2016).

[15] D. S. Jiang, X. P. Li, B. Q. Sun, et al. A Raman scattering study of GaAs:As films lifted off GaAs substrate, J. Phys. D: Appl. Phys., **32**, 629, (1999).

[16] M. Rocca. Plasmon-Phonon coupling in semiconductor. In: Chiarotti G., Chiaradia P. (eds) Physics of Solid Surfaces. Landolt-Börnstein - Group III Condensed Matter. Springer, Berlin, Heidelberg, **45A,** (2015).

[17] L. P. Avakyants, P. Y. Bokov, Optics and Spectroscopy **102**(5), 712, (2007).

[18] P. A. Grandt, A. E. Griffith, and M. O. Manasreha, Appl. Phys. Lett. **85**(21), 4905, (2004).

[19] R. Srnanek, Irmer G., D. Donoval, et al. Study of photoexcited plasma in p-doped GaAs beveled structures by micro-Raman spectroscopy, Applied Surface Science, **254**, 4845, (2008).

Acknowledgments

I would like to thank my supervisor Dr. Antonio Leyva for his limitless support and encouraging words, and to my friend Daina, without whom, in more than one way, this work would never have happened. Finally, I wish to thank the INTEREST Program at JINR for giving me this valuable opportunity to participate in this research project from one of the most important and prestigious nuclear physics institute in the world.